Journal of Nanostructure in Chemistry (2018) 8:441–452
https://doi.org/10.1007/s40097-018-0284-3

ORIGINAL RESEARCH

Adsorptive removal of cadmium from aqueous solutions using $NiFe_2O_4$/hydroxyapatite/graphene quantum dots as a novel nano-adsorbent

Parya Kahrizi[1] · Fatemeh S. Mohseni-Shahri[2] · Farid Moeinpour[2]

Received: 14 August 2018 / Accepted: 22 October 2018 / Published online: 16 November 2018

Abstract
In this study, $NiFe_2O_4$/hydroxyapatite/graphene quantum dots ($NiFe_2O_4$/HAP/GQDs) as nano-adsorbent to remove cadmium (Cd^{2+}) from aqueous solution were synthesized. This nano-adsorbent was depicted by some techniques such as X-ray diffraction (XRD), scanning electron microscopy (SEM), transmission electron microscopy (TEM) and Fourier transform infrared spectroscopy (FT-IR). Adsorption studies were conducted to investigate the effect of contact time, pH, adsorbent dosage and initial cadmium ion concentration on removal efficiency. To determine the most fitting kinetic model, the suitability of pseudo-first-order and pseudo-second-order models was compared. The adsorption isotherm was described well by the Langmuir isotherm and maximum equilibrium uptake capacity (q_e) was 344.83 mg g^{-1}. Studies revealed that adsorption process is not a physical process and formation of complexes (bidentate and monodentate complexes) between—COO^- and—OH functional groups on the surface of $NiFe_2O_4$/HAP/GQDs and Cd^{2+} ions may occur. In addition, the adsorbent can simply be removed by an ordinary filtration process.

Keywords Cd(II) ions removal · Graphene quantum dots · Nano-adsorbent · Isotherms

Introduction

Poisonous heavy metals like cadmium have been classified as the most destructive pollutants in the environment, because it is not degradable and highly harmful to health [1]. Cadmium has been shown to cause kidney failure [2]. Due to its hazardous impacts on human healthiness, removing cadmium from water and wastewater is a major environmental problem [3–6].

Different techniques have been used to remove metals from waters and wastewaters including ion exchange, reverse osmosis, chemical precipitation and electrolysis [7–11]. The above-mentioned methods have some disadvantages, for instance, time consuming, high cost, and secondary waste [12]. The use of nanotechnology is a major method for solving the problems of these methods [13–18]. Magnetic nanoparticles (NPs) have some unique properties such as great surface area, high adsorption capability, and rapid adsorption process. In last years, these materials have been more significant due to their particular characteristics. One of their specific characteristics is that almost all atoms are on the area of the nanoparticles. So, they can attach with more atoms that present superior chemical activity. Therefore, the nanoparticles can attract metal ions with a large adsorption rate [19]. Between different nanoparticles, hydroxyapatite (HAP) and graphene quantum dots (GQDs) are of great importance for their excellent usages. HAP ($Ca_{10}(PO_4)_6(OH)_2$) has been utilized for medical applications [20]. Considering its high specific surface area, slight solubility in water, numerous hydroxyl groups, availability, cheapness, environmental benign and easy synthesis method, it has been widely used as a sorbent for the removal of toxic elements from wastewaters [21].

GQDs, as a member of carbon-based nanomaterial, possess special properties including chemical inertness, slight toxicity, marvelous bio consistency, and excellent photo stability [22]. GQDs are graphene sheets similar to single, double and multiple layers all smaller than 10 nm deep and

✉ Fatemeh S. Mohseni-Shahri
f.mohseni@iauba.ac.ir; fmohsenishahri@gmail.com

[1] Department of Water and Wastewater Engineering, Bandar Abbas Branch, Islamic Azad University, Bandar Abbas, Iran

[2] Department of Chemistry, Bandar Abbas Branch, Islamic Azad University, Bandar Abbas 7915893144, Iran

100 nm in sideways size. Therefore, GQDs have ultrahigh specific surface area owing to the character of nano-sized graphene sheets; they have the ability for effective separation and removal of pollutants from environments. One can assume that by these types modified $NiFe_2O_4$ nanoparticles can improve the adsorption efficiency of cadmium.

In this project, a new magnetic nano-adsorbent, $NiFe_2O_4$/HAP/GQDs, was introduced to remove cadmium from aqueous solutions. Therefore, nano-adsorbent was synthesized (Scheme 1) and characterized by various techniques. Next, the properties of cadmium adsorption were investigated. Eventually, the efficacy of contact time, pH, $NiFe_2O_4$/HAP/GQDs dose and cadmium solution concentration on adsorption process was tested.

Materials and methods

Chemicals and reagents

Calcium nitrate tetrahydrate, sodium hydroxide, ammonium hydroxide, ferric nitrate 9-hydrate and nickel nitrate hexahydrate were obtained from Sigma-Aldrich. Acetic acid, hydrochloric acid and phosphoric acid were obtained from BDH. Paraffin oil was obtained from Iran paraffin Co. Cadmium sulfate hydrate was purchased from Merck Company of Germany. A 1000 mg L^{-1} stock solution of the salt was prepared in deionized water.

Instrumentation

The crystalline phase was tested by a diffractometer of the Philips Company with X'PertPro monochromatized Cu Kα radiation ($\lambda = 1.54$ Å). The microscopic structures and particle size were examined using SEM (Hitachi S-4800). Transmission electron microscopy (TEM) was carried out with a Leo 912AB (120 kV) microscope (Zeiss, Germany). FT-IR spectrum was specified on a Bruker model 470 spectrophotometer as KBr pellets. The magnetic characteristic was investigated by vibrating sample magnetometer (VSM, LDJ9600). The concentrations of cadmium ions were measured by an atomic absorption spectrophotometer (Varian AA240FS.)

Preparation of $NiFe_2O_4$/HAP/GQDs NPs

GQDs were prepared by pyrolysis of citric acid [23]. Concisely, 0.2 g of citric acid was added to a 100 ml round-bottomed flask and was heated at 200 °C for 5 min, until the white powder turned into a dark yellow viscous liquid. After the liquid was made, 20 ml of NaOH solution (0.25 M) was poured into a beaker, and while solution was stirred on the magnetic stirrer (at ambient temperature), the as-resulted liquid was added by pipette gradually into NaOH solution and allow to mix well together for 30 min. After 30 min, graphene dots were made and stored in a refrigerator (4 °C). 60 ml of egg white was poured into a beaker and mixed with 40 ml of distilled water. The mixture was stirred strongly at room temperature to completely mix each other and make a clear, uniform solution. Then 2.9081 g of $Ni(NO_3)_2{\cdot}6H_2O$ and 8.0800 g of $Fe(NO_3)_3{\cdot}9H_2O$ were added slowly to the previous solution and the solution was stirred strongly at laboratory temperature for 2 h until the salts were completely dissolved. In the next step, while stirring the solution, the solution was heated to 80° C for several hours until dried. The resulted powder was milled and calcined in a furnace at 700 °C for 3 h [24].

The dispersed $NiFe_2O_4$ in solution was then mixed with 10 mL $Ca(NO_3)_2.\ 4H_2O$ solution (0.835 mol L^{-1}) and 10 mL NH_4OH (28% w/v) to control pH close to 11. Next, 10 mL H_3PO_4 (0.5 mol L^{-1}) was added gradually (Ca/P molar ratio was about 1.67) [25]. After incubation at 80 °C for 30 min, the mixture was mixed with GQDs (20 mL) and stirred at 80 °C for 30 min.

Then, the resulting magnetic nanoparticles were cooled to room temperature and left for 2 h without stirring. The obtained solid was separated by a magnet; several steps were

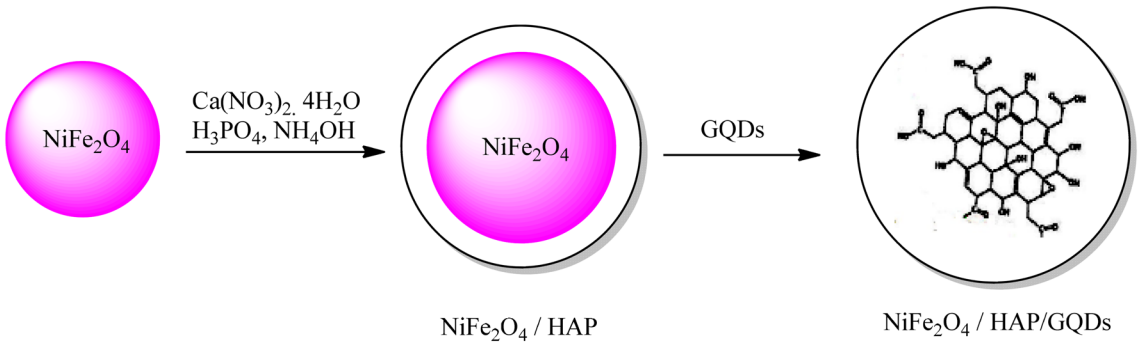

Scheme 1 Formation process of the $NiFe_2O_4$@HAP@GQDs nanocomposite

washed with water to neutralize and then dried at 90 °C, and crushed. Then, the $NiFe_2O_4$/HAP/GQDs were obtained.

Cadmium adsorption by $NiFe_2O_4$/HAP/GQDs

Adsorption of Cd^{2+} from aqueous solution by $NiFe_2O_4$/HAP/GQDs was examined in batch experiments. The effect of several effective parameters, i.e., reaction time, pH, adsorbent dosage and starting concentration was studied. In these experiments, all vessels were shaken at 200 rpm and at lab temperature (25 ± 1 °C). The pHs of solutions were regulated with proper concentrations of HCl and NaOH by a pH meter. Kinetic experiments were conducted with constant $NiFe_2O_4$/HAP/GQDs dose (0.1 g) at certain time intervals (1.0, 3.0, 5.0, 7.0, 10, 15, 20, 30, 40 and 60 min) at pH = 6. The uptake isotherm experiments were done by mixing 0.03 g of $NiFe_2O_4$/HAP/GQDs in a jar containing 100 mL of Cd^{2+} solutions with varying concentrations (5, 10, 20, 40, 50 and 100 mg L^{-1}) at pH = 6 for 10 min to reach equilibrium. Kinetic experiments demonstrated that contact time of 10 min was enough to attain equilibrium. So, this period of time was chosen for all isotherm experiments. After that, the nano-adsorbent was separated magnetically from solutions and then remaining cadmium concentration was measured by atomic absorption spectrophotometer. Then, amount of adsorbed per unit mass of adsorbent, q_e (mg g^{-1}), was calculated using Eq. (1) [26]:

$$q_e = \frac{C_0 - C_e}{M} \times V, \tag{1}$$

where C_0, C_e, V and M are initial Cd concentration (mg L^{-1}), equilibrium concentration of Cd (mg L^{-1}), volume of solution (L) and adsorbent dosage (g), respectively.

Results and discussion

Characterization of $NiFe_2O_4$/HAP/GQDs

The particle size of the $NiFe_2O_4$/HAP/GQDs was examined by the SEM and TEM. The SEM image of the $NiFe_2O_4$/HAP/GQDs in Fig. 1 reveals that the average size of adsorbent is about 25 nm. The TEM image of the $NiFe_2O_4$/HAP/GQDs in Fig. 2 shows that monotonous and compatible spherical shapes were achieved with an average diameter of about less than 25 nm. They were aggregated with several nanoparticles, and create a rough surface. Also, to analyze

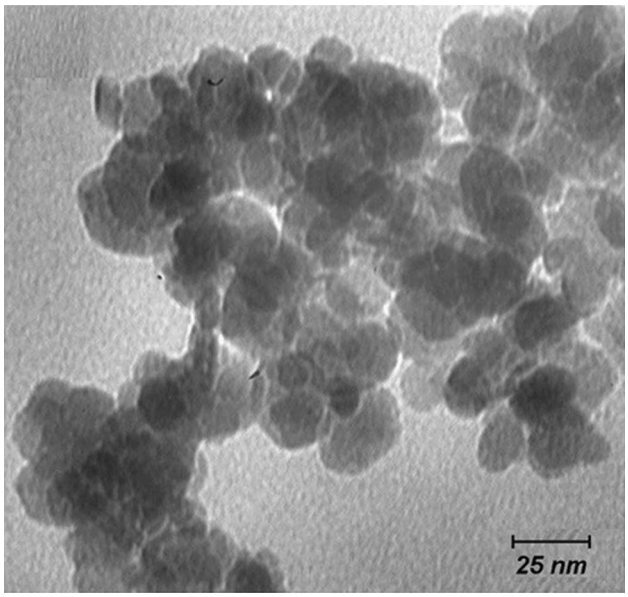

Fig. 2 TEM image of $NiFe_2O_4$/HAP/GQDs

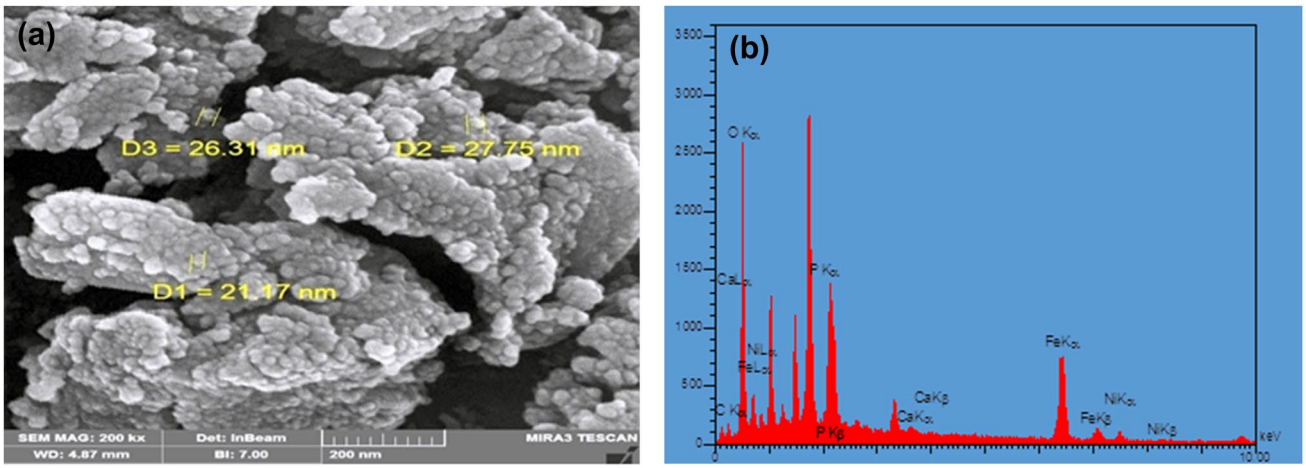

Fig. 1 SEM image (**a**) of $NiFe_2O_4$/HAP/GQDs and its EDX spectrum (**b**)

the relative amount of the principal elements of the $NiFe_2O_4$/HAP/GQDs nanocomposite containing Ni, Fe, O, Ca, P and C, EDX spectrum was handled to verify their elemental compositions (Fig. 1). According to EDX determinations, Fe (33.36%), Ni (2.64%), O (51.19%), Ca (2.37%), P (1.44%) and C (6.49%) were present in $NiFe_2O_4$/HAP/GQDs. The Ca:P ratio calculated from the EDX was 1.65 which is near to the stoichiometric ratio (1.67) that occurs in the natural hydroxyapatite [27, 28]. This showed that the hydroxyapatite was formed with the suggested process.

The FT-IR spectra of $NiFe_2O_4$, $NiFe_2O_4$/HAP, and $NiFe_2O_4$/HAP/GQDs are illustrated in Fig. 3. In FT-IR spectra, there are two typical peaks at 555 and 1440 cm^{-1} are correlated with Fe–O vibrations [29]. The bands approximately 971 and 1116 cm^{-1} are due to stretching mode of phosphate (P–O, PO_4^{3-}) [30]. They are the main attributes of HAP bands. The absorption band appearing around 3300 cm^{-1} represents O–H vibrations. Moreover, the peak located at 3100 cm^{-1} in spectrum indicates the asymmetric stretching and symmetric vibrations of C–H. The occurrence of the C=C bending vibrations peak at 1574 cm^{-1} and C=O stretching vibration band at 1668 cm^{-1} gives a strong proof of GQDs and synthesis of $NiFe_2O_4$/HAP/GQDs [31].

To verify the formation of $NiFe_2O_4$ in the prepared nanocomposite, the XRD patterns of the samples were investigated (Fig. 4). The XRD patterns (Fig. 4a) confirm that these nanoparticles are spinel shaped, and all of the main peaks corresponding the standard pattern of bulk $NiFe_2O_4$ (JCPDS 08-0234). Additionally, the existence of hydroxyapatite is proved in Fig. 4b. As can be shown in Fig. 4c, no signal about GQDs can be detected,

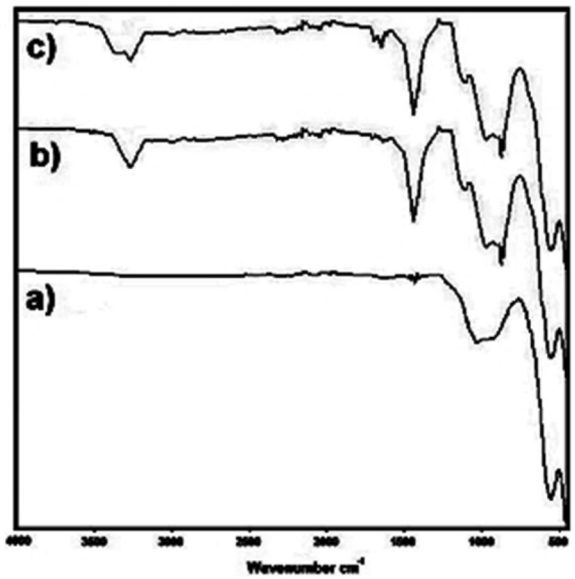

Fig. 3 FT-IR spectra of $NiFe_2O_4$ (**a**), $NiFe_2O_4$/HAP (**b**), and $NiFe_2O_4$/HAP/GQDs (**c**)

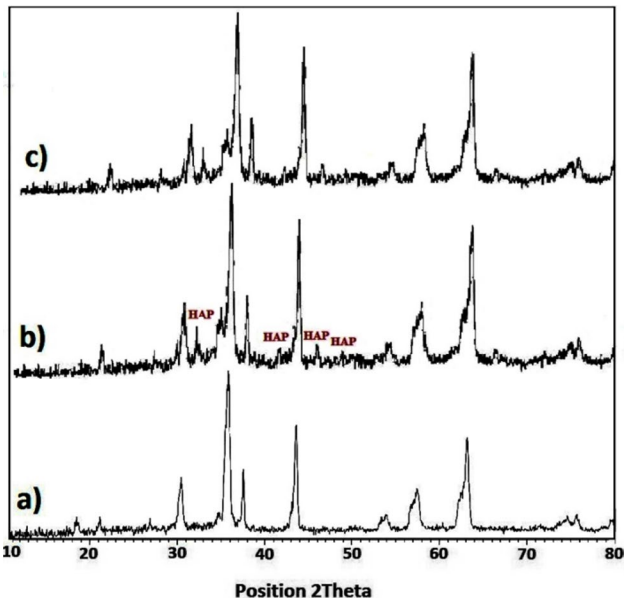

Fig. 4 XRD patterns of $NiFe_2O_4$ (**a**), $NiFe_2O_4$/HAP (**b**), and $NiFe_2O_4$/HAP/GQDs (**c**)

which is described by the small amounts, high dispersion and low crystallinity of GQDs in $NiFe_2O_4$/HAP/GQDs nanocomposite.

The magnetic characteristics of the $NiFe_2O_4$/HAP/GQDs nanocomposite were identified using vibrating sample magnetometer (VSM). As can be seen in Fig. 5, M(H) hysteresis loop was completely reversible for the sample, indicating that the $NiFe_2O_4$/HAP/GQDs nanocomposite shows superparamagnetic characteristics. The hysteresis loops of them reached saturation up to the ultimate applied magnetic field. At room temperature, the magnetic saturation value of the $NiFe_2O_4$/HAP/GQDs is 24.88 emu g^{-1}. The high permeability of particles in the magnetization showed that they could be separated by a typical magnetometer.

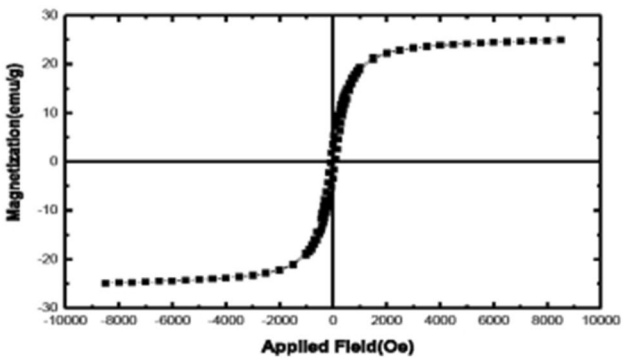

Fig. 5 Magnetization curve of the $NiFe_2O_4$/HAP/GQDs nanocomposite at room temperature

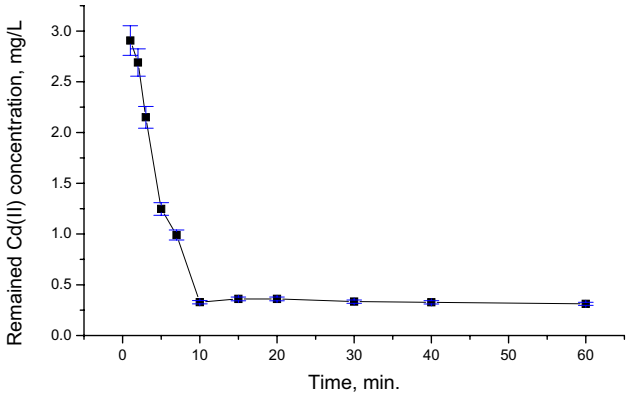

Fig. 6 Effect of contact time on % Cd(II) ions removal efficiency (initial pH = 6, initial Cd(II) ions concentration = 10 mg L^{-1}, adsorbent dose = 0.1 g/100 mL and temperature = 25 °C)

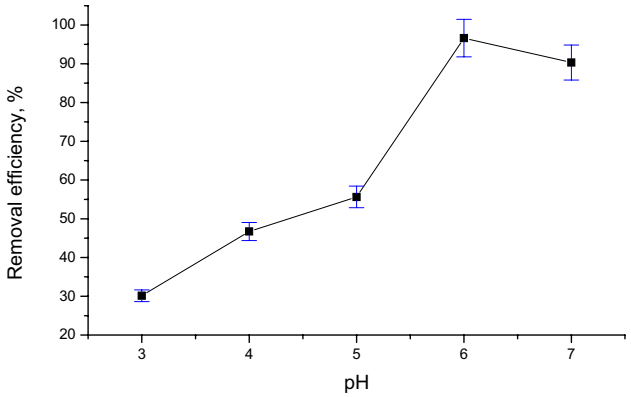

Fig. 7 Effect of pH on % Cd(II) ions removal efficiency (contact time = 10 min., initial Cd(II) ions concentration = 10 mg L^{-1}, adsorbent dose = 0.1 g/100 mL and temperature = 25 °C)

Effect of contact time

The impact of contact time on the Cd^{2+} adsorption value by $NiFe_2O_4$/HAP/GQDs was studied at 10 mg L^{-1}, to optimize the adsorption time and to investigate the kinetics of the uptake process. As contact time enhances, the concentration of Cd^{2+} in the solution reduced quickly at first and later decelerates until it stayed constant at around 10 min, which was taken as the equilibrium time (Fig. 6). The adsorption specification suggested a rapid uptake of the cadmium. The fast level of Cd^{2+} adsorption at the initial minutes of adsorption process may be owing to the great number of empty sites accessible at the early period of the adsorption [32].

Effect of pH

The acidic property of a solution is one of the determining factors in the uptake process, specifically adsorption capacity [29]. To assess the impact of pH on the removal efficiency, the tests were accomplished in the pH range of 3–7. The results are shown in Fig. 7.

In lower pHs, high concentrations of hydrogen ions exist and, based on the theory of surface complex formation, hydrogen ions are absorbed instead of the metal ions.

So, as shown in Fig. 6 the removal of Cd^{2+} in low pHs is slighter than that of in high-level pHs. The amount of Cd^{2+} adsorbed increased with increasing the pH value of solution from 3 to 6.0 (approximately); this aspect can be interpreted by precipitation of Cd^{2+} as insoluble $Cd(OH)_2$ precipitate. In other words, in these pH values (˃ 6), the Cd(II) ions begin to hydrolyze and then form a small quantity of cadmium hydroxyl species [33]. In other words, at lower pH (less than 3), the low metal adsorption can be assigned to the protonated surfaces of $NiFe_2O_4$/HAP/GQDs, electron repulsion, and competition between Cd^{2+} and H^+ ions. For the pH ranges from 3 to 6, the equilibrium absorption of Cd (II) ions increased dramatically as the pH increased.

This treatment can be attributed to a reduction in the amount of protonation by increasing the pH, which minimizes the competition between H^+ and Cd^{2+}ions on active sites and increase the Cd(II) ions. Additional increment in solution pH, beyond 7, brings about precipitation of cadmium as cadmium hydroxide. In comparison with Cd(II) ions, these species are undesirable for adsorption, which is a reason for a slight reduction in removal efficiency percent and adsorption capacity. Thus, the maximum absorption was around pH 6.0, and therefore selected for all absorption experiments in this study.

Effect of adsorbent dosage

The uptake productivity rises with enhancing adsorbent dosage on the adsorption processes. It is of vital importance to achieve the best removal efficiency with low adsorbent dose as possible. Therefore, the most efficient adsorbent dose measurement for adsorption processes is necessary. The effect of the adsorbent dosage was investigated by repeating experiments with different adsorbent dosage (from 0.01 to 0.2 g/100 mL). Accordingly, the values of other parameters were applied as contact time 10 min, the initial pH value of solution 6, initial Cd(II) ions concentrations 10 mg L^{-1}, and temperature 25 °C. The outcomes are illustrated in Fig. 8. According to the results obtained from this study, the adsorption efficacy increased significantly with rising adsorbent dosage. As adsorbent amount in solution is increased, the removal efficiency also rapidly rises. The greatest removal efficiency was found to be 97.6% at the adsorbent mass of 0.03 g/100 mL. The increase in cadmium removal with increasing adsorbent dosage can be ascribed to enhanced surface area and the adsorption sites. This situation may be explained by the fact that the higher the concentrations of

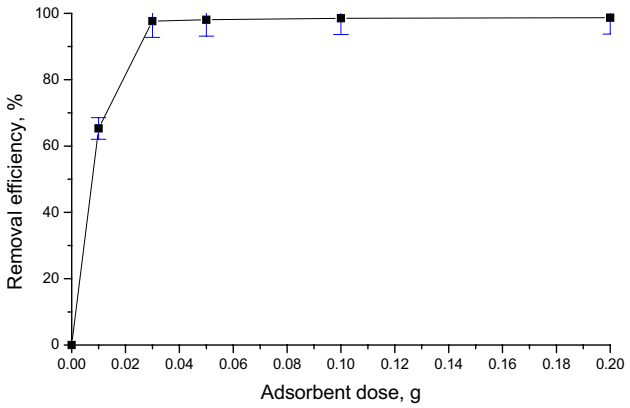

Fig. 8 Effect of adsorbent dosage on % Cd(II) ions removal efficiency (contact time = 10 min., initial pH = 6, initial Cd(II) ions concentration = 10 mg L^{-1} and temperature = 25 °C)

adsorbent, the more sorbent surface and pore volume will be accessible for the adsorption (Fig. 8).

Effect of initial Cd(II) ions concentration

Batch adsorption tests were carried out at various initial Cd^{2+} concentrations (5, 10, 20, 40, 50, 100, 200 and 300 mg L^{-1}), at pH 6. 0.03 g/100 mL of $NiFe_2O_4$/HAP/GQDs was used for each adsorption test, with a contact time of 10 min. Figure 9 illustrated that with a rise in the initial cadmium concentration from 5.0 to 300 mg L^{-1}, the amount of cadmium adsorption decreased. Removal percentage was greater for low initial Cd^{2+} concentration owing to accessibility of vacant binding sites on the adsorbent. Since, at high Cd^{2+} concentrations the binding sites were approximately entirely covered, removal efficiency decreased with increasing metal concentration.

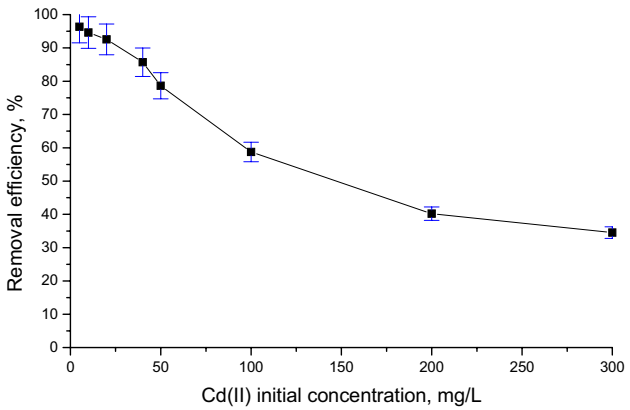

Fig. 9 Effect of initial Cd(II) ions concentration on % Cd(II) ions removal efficiency (contact time = 10 min., initial pH = 6, adsorbent dose = 0.03 g/100 mL and *t* Fig. 11 The Langmuir (**a**), Freundlich (**b**) and Dubinin – Radushkevich (**c**) isotherms for the Cd^{2+} on the $NiFe_2O_4$/HAP/GQDs surface

Effect of ionic strength

To investigate the effect of ionic strength on the efficiency of removal of Cd(II) by $NiFe_2O_4$/HAP/GQDs, tests were conducted under optimum conditions, and five different times (5, 10, 20, 30 and 60 min) with three different ionic strengths (0.1, 0.3 and 3 mol L^{-1}). The ionic strength in each experiment was set using sodium sulfate. The results of each experiment are calculated and shown in Fig. 10. The ionic strength of the solution in the adsorption process of cadmium ions is very important. Because solutions with high ionic strength are similar and comparable to wastewaters, such solutions result in more absorption through electromagnetic interactions between cadmium ions and adsorbent surface. In accord with the surface chemistry theory, when $NiFe_2O_4$/HAP/GQDs is in contact with Cd(II) ions in solution, they are encircled by an electrical diffused double layer, the thickness of which is remarkably extended in the presence of electrolyte [34]. In this study, to evaluate the effect of ionic strength on the adsorption process by $NiFe_2O_4$/HAP/GQDs, the ability of three different ionic strengths (0.1, 0.3 and 3 mol L^{-1}) were chosen. As Fig. 10 displays, with rising of ionic strength from 0.1 to 3 mol L^{-1}, Cd(II) ions removal efficiency reduces. This phenomenon occurs because increasing the concentration of sodium ions in the solution increases the ionic strength of the solution too. The sodium ions are located near the surface of $NiFe_2O_4$/HAP/GQDs. The aggregation of these positive ions throughout the adsorbent leads to a reduction in the exposure between Cd(II) ions and $NiFe_2O_4$/HAP/GQDs and finally, Cd(II) ions adsorption capability by the adsorbent reduces. On the other hand, the high concentration of sodium ions competes with Cd^{2+} ions and place on the active sites present on the surface

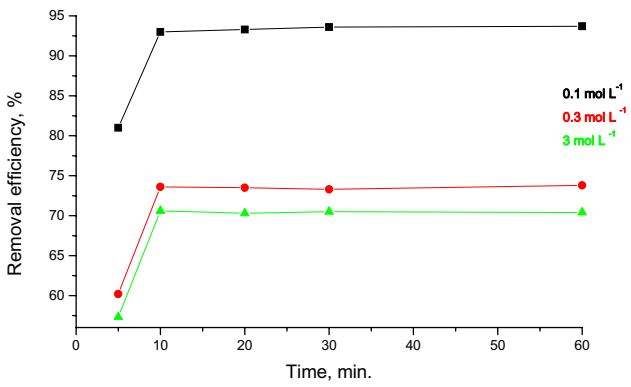

Fig. 10 Effect of the ionic strength on % Cd(II) ions removal efficiency (initial pH = 6, initial Cd(II) ions concentration = 10 mg L^{-1} and temperature = 25 °C)

of $NiFe_2O_4$/HAP/GQDs. Therefore, the active sites on the surface of the $NiFe_2O_4$/HAP/GQDs fill completely and cause a reduction in Cd(II) ions removal efficiency.

Adsorption isotherms

An adsorption isotherm model shows the equilibrium correlation between the absorption of matter per unit mass of adsorbent at constant temperature and its concentration in solution [35, 36]. The experimental outcomes of this study were investigated by Langmuir, Freundlich and Dubinin–Radushkevich (D–R) models, as indicated in Table 1 and Fig. 11.

The Langmuir isotherm model, which proposes that adsorption takes place at homogeneous sites by monolayer uptake with no considerable interaction between adsorbed ions, is given as follows:

$$\frac{C_e}{q_e} = \frac{1}{K_L}\frac{1}{q_m} + \frac{1}{q_m}C_e, \tag{2}$$

where q_e is the value of Cd^{2+} adsorbed per unit mass at equilibrium (mg g^{-1}), q_m denotes the maximum value of adsorbent that can be adsorbed per unit mass adsorbent (mg g^{-1}), C_e is the concentration of adsorbent in the solution at equilibrium (mg L^{-1}) and K_L (L mg^{-1}) represents the Langmuir isotherm constant. A linear plot of C_e/q_e against C_e, yields a straight line with a slope of $1/q_m$ and an intercept of $1/K_L q_m$ [37].

The main features of the Langmuir isotherm can be stated in terms of a dimensionless constant separation factor R_L which is defined as [38]:

$$R_L = \frac{1}{1 + K_L C_0}, \tag{3}$$

where C_0 the initial concentration of Cd^{2+} ions (mg L^{-1}), and K_L (L mg^{-1}) is the Langmuir constant. The amount of R_L indicates the shape of the isotherm to be either unfavorable

Table 1 Langmuir, Freundlich, D–R isotherm constants for the adsorption of Cd (II) ions onto $NiFe_2O_4$/HAP/GQDs

Langmuir	q_m (mg g^{-1})	344.83
	KL	0.076
	RL	0.042
	R^2	0.9704
Freundlich	1/*n*	0.415
	KF	42.761
	R^2	0.9704
Dubinin–Radushkevich (D–R)	q_m (mg g^{-1})	153.35
	β (mol^2 kJ^{-2})	1×10^{-7}
	R^2	0.707
	E (kJ mol^{-1})	2.24

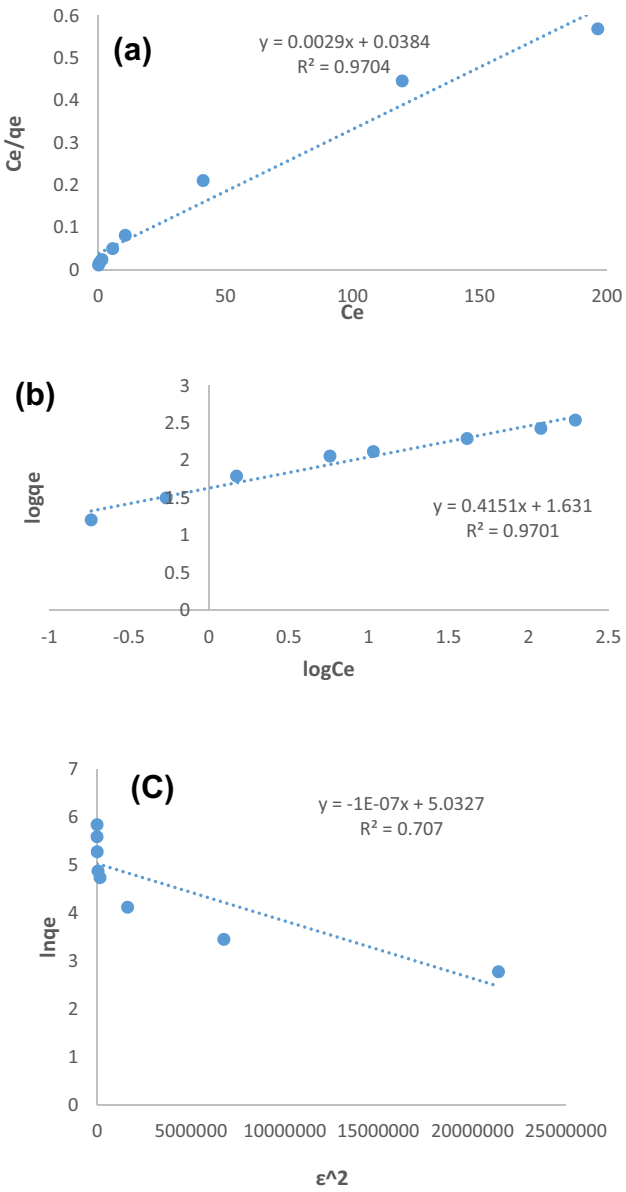

Fig. 11 The Langmuir (**a**), Freundlich (**b**) and Dubinin – Radushkevich (**c**) isotherms for the Cd^{2+} on the $NiFe_2O_4$/HAP/GQDs surface

($R_L > 1$), linear ($R_L = 1$), favorable ($0 < R_L < 1$), or irreversible ($R_L < 0$). In this study, the value of R_L is 0.042 and shows the favorable adsorption between $NiFe_2O_4$/HAP/GQDs and Cd^{2+}.

The Freundlich isotherm is used for heterogeneous adsorption with various surface energy sites and considers the alteration of adsorption with exponential distribution of adsorption sites and energies. The Freundlich model is represented as follows [39]:

$$\log q_e = \log K_F + \frac{1}{n}\log C_e, \tag{4}$$

where q_e is the amount of adsorbent adsorbed per unit mass of adsorbent (mg g^{-1}), C_e denotes the equilibrium concentration of adsorbent in the solution (mg L^{-1}), K_F ($mg^{1-(1/n)}$ $L^{1/n}$ g^{-1}) and n depict Freundlich constants which indicate the uptake capacity for the adsorbent and uptake intensity, respectively. Freundlich parameters K_F and n can be calculated from the intercept and slope of a linear plot with $\log q_e$ versus $\log C_e$.

If the value of $1/n < 1$, then the adsorption intensity and the type of isotherm to be desirable and the adsorption capacity rise with the appearance of new adsorption sites. But if $1/n > 1$, the absorption bond weakens and its absorption is very difficult, which reduces the absorption capacity. In this study, the value of 1/n (0.415) displays the favorable adsorption of Cd^{2+}on $NiFe_2O_4$/HAP/GQDs.

Dubinin–Radushkevich (D–R) equation was used to determine whether chemical or physical absorption was observed. This equation defined as:

$$\ln q_e = \ln q_m - \beta\varepsilon^2, \tag{5}$$

where q_m is the maximum adsorption capacity of metal ions (mg g^{-1}), β is a constant related to the mean energy of adsorption (mol^2 kJ^{-2}), ε is the Polanyi potential given as follows:

$$\varepsilon = \mathrm{RTln}\left(1 + \frac{1}{C_e}\right), \tag{6}$$

where T is the temperature (K) and R is the gas constant (8.314 J K^{-1} mol^{-1}). A linear plot of

ln q_e against ε^2, gives a straight line with a slope of and an intercept of ln q_m. With the value of β, the mean energy E, which is the free energy transfer of one mole of solute from infinity to absorbing surface, can be evaluated by Eq. (7):

$$E = \frac{1}{\sqrt{2\beta}}. \tag{7}$$

If $E < 8$ kJ mol^{-1}, then the adsorption process might be performed physically, but if $E > 8$ kJ mol^{-1} chemical adsorption may occur [40].

Table 1 shows the values of Langmuir, Freundlich and (D–R) constants and the correlation coefficients obtained from the linear regression. Based on the results, it can be derived from R^2 that both Langmuir and Freundlich models hold high linearity as they are very close to each other. Thus, two criterions (MSE and χ^2) were used to check the accuracy of the Langmuir and Freundlich models as calculated by following equations [41]:

$$\mathrm{MSE} = \frac{1}{n}\sum_{n=1}^{n}\left(q_{exp} - q_{cal}\right)^2, \tag{8}$$

$$\chi^2 = \frac{\sum_{n=1}^{n}\left(q_{exp} - q_{cal}\right)^2}{q_{cal}}, \tag{9}$$

where q_{exp} and q_{cal} represent the experimental and calculated uptake values, respectively (mg g^{-1}).

Table 2 shows that the Langmuir model has low values of MSE and χ^2, while the Freundlich model has the highest error rate. These results supported the validity of the Langmuir model for the absorption process. Although both models were almost identical to R^2, there was a significant difference in MSE and χ^2 values between the two models, which indicates that R^2 can be used only for the use of the trend, and the two equal values of R^2 inevitably mean errors are not the same.

From the Table 1, it is denoted that the predicted q_m value from D–R isotherm is not conforming with the formerly determined Langmuir isotherm q_m value. The correlation coefficient for the D–R isotherm is lower than the values of the two isotherm models (Table 1), which indicates that the Cd(II) ions uptake on $NiFe_2O_4$/HAP/GQDs is not a physical process [42].

Table 2 Results of models error calculation at room temperature

Model	R^2	MSE	χ^2
Langmuir	0.9704	0.0005	0.018
Freundlich	0.9701	0.1120	0.589

Adsorption kinetics

Different kinetic models are proposed for precise design of the absorption process [32, 43]. In this study, the equations of Lagergren's pseudo-first-order kinetic model and Ho's pseudo-second-order kinetic model were used. The pseudo-first order model is given as [44]:

Table 3 Kinetic model parameters for the Cd(II) ions adsorption on $NiFe_2O_4$/HAP/GQDs

Kinetic models						
Pseudo-first order			Pseudo-second order			
R^2	$q_{e,cal}$ (mg g^{-1})	k_1 (min^{-1})	R^2	q_e, exp. (mg g^{-1})	q_e, cal.(mg g^{-1})	k_2 (g/(mg.min))
0.949	13.010	0.2796	0.999	32.238	32.573	0.0698

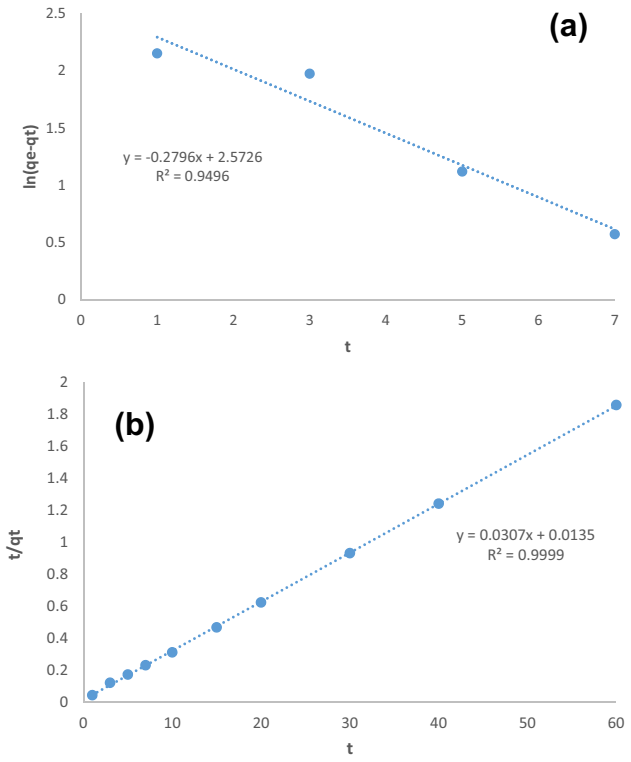

Fig. 12 Kinetic curves: pseudo--first-order model (**a**) and pseudo-second-order model (**b**)

$$\ln\left(q_e - q_t\right) = \ln q_e - k_1 t, \tag{10}$$

where q_e and q_t (mg g^{-1}) are the adsorption capacities at equilibrium and at time t (min), respectively. k_1 (min^{-1}) is the rate constant for the pseudo-first-order model.

The pseudo-second-order equation is defined as [45]:

$$\frac{t}{q_t} = \frac{1}{k_2 q_e^2} + \frac{t}{q_e}, \tag{11}$$

where k_2 (g mg^{-1} min^{-1}) is the rate constant for the pseudo-second-order rate equation, and other symbols have their usual meanings. The amounts of q_e and k_2 can be derived from the slope and intercept of the plot of t/q_t versus t. The kinetics parameters of the pseudo-first- and pseudo-second-order models and their corresponding coefficients of correlation, R^2, are indicated in Table 3 and Fig. 12.

The results of Table 3 showed that the correlation coefficient was very high ($R^2 = 0.999$). Additionally, the calculated equilibrium absorption capacity was consistent with experimental results. This result showed that kinetic data were better arranged with a pseudo-second kinetic model. Based on the pseudo-second order model, the chemical absorption is a limiting step, so reliable results suggest that the absorption behavior may be in the sharing of electrons or exchange between the Cd^{2+} ions and $NiFe_2O_4$/HAP/GQDs. Similar findings have been reported for the absorption of Cd^{2+} ions [46, 47]. Therefore, the results from the interpretation of isotherms are consistent with the results of kinetics studies.

Considering the above results, the Cd^{2+} adsorption by $NiFe_2O_4$/HAP/GQDs probably can occur in the pathway

Scheme 2 Possible adsorption mechanism of Cd^{2+} onto $NiFe_2O_4$/HAP/GQDs Surface

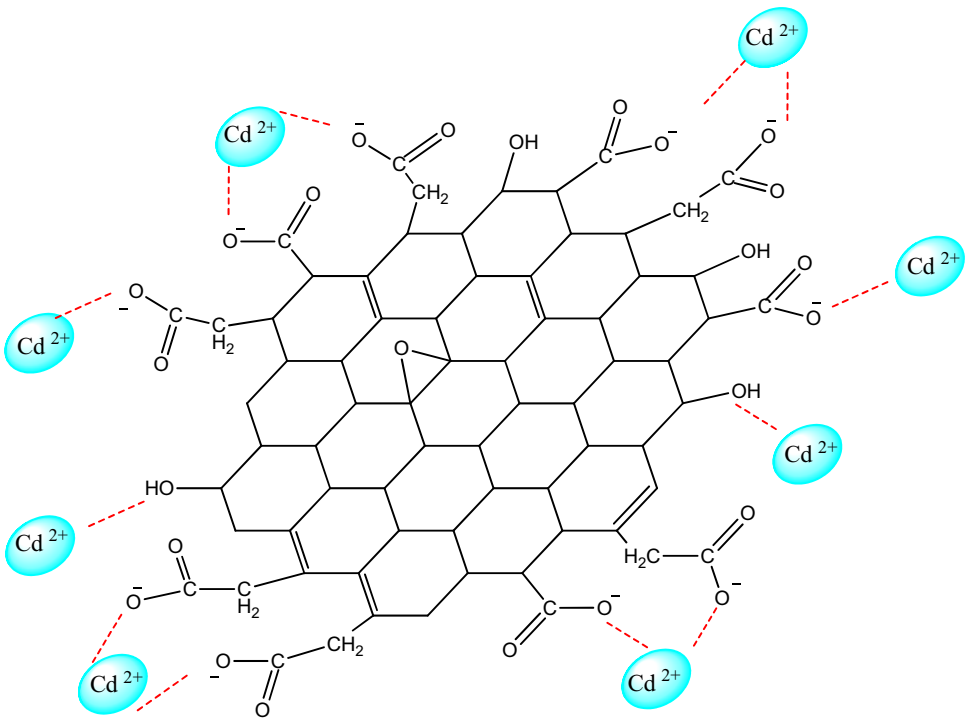

Table 4 Maximum adsorption capacity of different adsorbents for Cd(II) ions removal

Adsorbents	q_m (mg g^{-1})	References
Fe_3O_4 nanoparticles-loaded sawdust carbon	51	[51]
Bamboo powder	8.57	[52]
Burmese grape leaf extract	44.72	[53]
Magnesium silicate–hydrothermal carbon composite	108	[54]
Aminothiourea chitosan–modified magnetic biochar composite	93.72	[55]
Sulfur-functionalized rice husk	137.16	[56]
Nano-Pumice	200	[45]
$NiFe_2O_4$/HAP/GQDs	344.83	Present study

[48–50], which was demonstrated in Scheme 2. The formation of complexes (bidentate and monodentate complexes) between $–COO^{—}$ and –OH functional groups on the surface of $NiFe_2O_4$/HAP/GQDs and Cd^{2+} ions has been occurred. Generally, the results showed that in this study the main route in the adsorption process between $NiFe_2O_4$/HAP/GQDs and Cd^{2+} may be chemical absorption.

Absorption capacity is an important parameter that determines the behavior of an adsorbent. Table 4 compares the maximum absorption capacity of $NiFe_2O_4$/HAP/GQDs for Cd(II) ions and other adsorbents in previous publications.

As shown in Table 4, the experimental data of the present study are comparable with the reported values in some cases. The absorption capacity varies and depends on the individual absorbent properties, the extent of surface/surface modification and the initial concentration of the adsorbate. However, current experiments are conducted to find a low-cost absorbent for Cd(II) treatment.

Conclusion

The results of present study show that the $NiFe_2O_4$/HAP/GQDs nano-adsorbent could be successfully used to remove cadmium ions from aqueous solutions. The results indicate that HAP/GQDs have been supported well on the $NiFe_2O_4$. The derived outcomes revealed that the equilibrium time for the adsorption of the cadmium ions onto adsorbent was 10 min and the most efficient condition for removal of cadmium at pH = 6.0 was obtained with a maximum absorption capacity of 344.83 mg g^{-1} at 25 °C. Increasing the concentration of cadmium reduced the absorption of the nano-adsorbent. The Langmuir isotherm model was more suitable than Freundlich isotherm for determining the equilibrium.

The kinetic studies show that the absorption process is well arranged by a pseudo-second-order kinetic model. Accordingly, $NiFe_2O_4$/HAP/GQDs nano-adsorbent is an effective absorbent adsorbent and can be used as a useful and valuable agent for removing cadmium ions from aqueous solutions.

Acknowledgements The authors appreciate the Islamic Azad University-Bandar Abbas Branch for financial support of this study.

References

1. Zeng, G., Pang, Y., Zeng, Z., Tang, L., Zhang, Y., Liu, Y., Zhang, J., Lei, X., Li, Z., Xiong, Y., Xie, G.: Removal and recovery of Zn^{2+} and Pb^{2+} by imine-functionalized magnetic nanoparticles with tunable selectivity. Langmuir **28**, 468–473 (2011)
2. Jean, J., Sirot, V., Hulin, M., Le Calvez, E., Zinck, J., Noël, L., Vasseur, P., Nesslany, F., Gorecki, S., Guérin, T., Rivière, G.: Dietary exposure to cadmium and health risk assessment in children–results of the French infant total diet study. Food Chem. Toxicol. **115**, 358–364 (2018)
3. Govender, S., Przybylowicz, W., Swart, P.: Removal of heavy metals from solution using biocompatible polymers. Desalin. Water Treat. **9**, 272–278 (2009)
4. Shamohamadi, S., Bustanian, M., Tavakol, H.: Removing Cd^{2+} from water and wastewater by blowy sand; the effects of total hardness and pH. Desalin. Water Treat. **51**, 3463–3471 (2013)
5. Mhamdi, M., Elaloui, E., Trabelsi-Ayadi, M.: Kinetics of cadmium adsorption by smectite of Oued Tfal (Gafsa Basin). Desalin. Water Treat. **52**, 4245–4256 (2014)
6. Yang, G., Tang, L., Lei, X., Zeng, G., Cai, Y., Wei, X., Zhou, Y., Li, S., Fang, Y., Zhang, Y.: Cd(II) removal from aqueous solution by adsorption on α-ketoglutaric acid-modified magnetic chitosan. Appl. Surf. Sci. **292**, 710–716 (2014)
7. Lee, S.M., Laldawngliana, C., Tiwari, D.: Iron oxide nanoparticles-immobilized-sand material in the treatment of Cu(II), Cd(II) and Pb(II) contaminated waste waters. Chem. Eng. J. **195**, 103–111 (2012)
8. Gong, R., Cai, W., Li, N., Chen, J., Liang, J., Cao, J.: Preparation and application of thiol wheat straw as sorbent for removing mercury ion from aqueous solution. Desalin. Water Treat. **21**, 274–279 (2010)
9. Yogesh Kumar, K., Muralidhara, H.P., Arthoba Nayaka, Y., Balasubramanyam, J.: Low-cost synthesis of mesoporous Zn (II) – Sn (II) mixed oxide nanoparticles for the adsorption of dye and heavy metal ion from aqueous solution. Desalin. Water Treat. **52**, 4568–4582 (2014)

10. Tang, L., Yang, G., Zeng, G.M., Cai, Y., Li, S.S., Zhou, Y., Pang, Y., Liu, Y.Y., Zhang, Y., Luna, B.: Synergistic effect of iron doped ordered mesoporous carbon on adsorption-coupled reduction of hexavalent chromium and the relative mechanism study. Chem. Eng. J. **239**, 114–122 (2014)
11. Li, J., Wang, X., Zhao, G., Chen, C., Chai, Z., Alsaedi, A., Hayat, T., Wang, X.: Metal–organic framework-based materials: superior adsorbents for the capture of toxic and radioactive metal ions. Chem. Soc. Rev. **47**, 2322–2356 (2018)
12. Acharya, J., Kumar, U., Rafi, P.M.: Removal of Heavy metal ions from wastewater by chemically modified agricultural waste material as potential adsorbent-a review. Int. J. Curr. Trends Eng. Technol. **8**, 526–530 (2018)
13. Zhao, G., Li, J., Ren, X., Chen, C., Wang, X.: Few-layered graphene oxide nanosheets as superior sorbents for heavy metal ion pollution management. Environ. Sci. Technol. **45**, 10454–10462 (2011)
14. Gu, P., Zhang, S., Li, X., Wang, X., Wen, T., Jehan, R., Alsaedi, A., Hayat, T., Wang, X.: Recent advances in layered double hydroxide-based nanomaterials for the removal of radionuclides from aqueous solution. Environ. Pollut. **240**, 493–505 (2018)
15. Zhao, G., Huang, X., Tang, Z., Huang, O., Niu, F., Wang, X.: Polymer-based nanocomposites for heavy metal ions removal from aqueous solution: a review. Polym. Chem. **9**, 3562–3582 (2018)
16. Siddiqui, S.I., Chaudhry, S.A.: Nigella sativa plant based nanocomposite-MnFe2O4/BC: an antibacterial material for water purification. J. Clean. Prod. **200**, 996–1008 (2018)
17. Siddiqui, S.I., Chaudhry, S.A., Islam, S.: Green adsorbents from plant sources for the removal of arsenic an emerging wastewater treatment technology. In: Islam, S.U. (ed.) Plant-based natural products derivatives and applications, pp. 193–215. Wiley, Hoboken (2017)
18. Siddiqui, S.I., Ravi, R., Rathi, G., Tara, N., ul-Islam, S.: Decolorization of textile wastewater using composite materials. In: Islam, S.U., Butola, B.S. (eds.) Nanomaterials in the wet processing of textiles, pp. 187–218. Wiley, Hoboken (2018)
19. Zhai, Y., Chang, X., Cui, Y., Lian, N., Lai, S., Zhen, H., He, Q.: Selective determination of trace mercury (II) after preconcentration with 4-(2-pyridylazo)-resorcinol-modified nanometer-sized SiO_2 particles from sample solutions. Microchim. Acta **154**, 253–259 (2006)
20. Zou, Z., Lin, K., Chen, L., Chang, J.: Ultrafast synthesis and characterization of carbonated hydroxyapatite nanopowders via sonochemistry-assisted microwave process. Ultrason. Sonochem. **19**, 1174–1179 (2012)
21. Saber-Samandari, S., Gazi, M.: Cellulose-graft-polyacrylamide/hydroxyapatite composite hydrogel with possible application in removal of Cu (II) ions. React. Funct. Polym. **73**, 1523–1530 (2013)
22. Hallaj, T., Amjadi, M., Manzoori, J.L., Shokri, R.: Chemiluminescence reaction of glucose-derived graphene quantum dots with hypochlorite, and its application to the determination of free chlorine. Microchim. Acta **182**, 789–796 (2015)
23. Benítez-Martínez, S., Valcárcel, M.: Fluorescent determination of graphene quantum dots in water samples. Anal. Chim. Acta **896**, 78–84 (2015)
24. Maensiri, S., Masingboon, C., Boonchom, B., Seraphin, S.: A simple route to synthesize nickel ferrite ($NiFe_2O_4$) nanoparticles using egg white. Scripta Mater. **56**, 797–800 (2007)
25. Brundavanam, R.K., Jiang, Z.T., Chapman, P., Le, X.T., Mondinos, N., Fawcett, D., Poinern, G.E.J.: Effect of dilute gelatine on the ultrasonic thermally assisted synthesis of nano hydroxyapatite. Ultrason. Sonochem. **18**, 697–703 (2011)
26. Awual, M.R., Khraisheh, M., Alharthi, N.H., Luqman, M., Islam, A., Karim, M.R., Rahman, M.M., Khaleque, M.A.: Efficient detection and adsorption of cadmium (II) ions using innovative nano-composite materials. Chem. Eng. J. **343**, 118–127 (2018)
27. Dil, E.A., Ghaedi, M., Asfaram, A.: The performance of nanorods material as adsorbent for removal of azo dyes and heavy metal ions: application of ultrasound wave, optimization and modeling. Ultrason. Sonochem. **34**, 792–802 (2017)
28. Sricharoen, P., Limchoowong, N., Techawongstien, S., Chanthai, S.: A novel extraction method for-carotene and other carotenoids in fruit juices using air-assisted, low-density solvent-based liquidliquid microextraction and solidified floating organic droplets. Food Chem. **15**, 386–393 (2015)
29. Pol, V.G., Thiyagarajan, P., Calderon Moreno, J.M., Popa, M.: Solvent-free fabrication of ferromagnetic Fe_3O_4 octahedra. Ind. Eng. Chem. Res. **49**, 920–924 (2009)
30. Moeinpour, F., Khojastehnezhad, A.: Cesium carbonate supported on hydroxyapatite coated $Ni_0.5Zn_0.5Fe_2O_4$ magnetic nanoparticles as an efficient and green catalyst for the synthesis of pyrano [2, 3-c] pyrazoles. Chin. Chem. Lett. **26**, 575–579 (2015)
31. Alvand, M., Shemirani, F.: A Fe_3O_4@ SiO_2@ graphene quantum dot core-shell structured nanomaterial as a fluorescent probe and for magnetic removal of mercury (II) ion. Microchim. Acta **184**, 1621–1629 (2017)
32. Yousef, R.I., El-Eswed, B., Ala'a, H.: Adsorption characteristics of natural zeolites as solid adsorbents for phenol removal from aqueous solutions kinetics, mechanism, and thermodynamics studies. Chem. Eng. J. **171**, 1143–1149 (2011)
33. Omidvar-Hosseini, F., Moeinpour, F.: Removal of Pb(II) from aqueous solutions using Acacia Nilotica seed shell ash supported $Ni_0.5Zn_0.5Fe_2O_4$ magnetic nanoparticles. J. Water Reuse Desal. **6**, 562–573 (2016)
34. Osipow, L.I.: Surface chemistry: theory and industrial applications. Reinhold Pub, New York (1962)
35. Siddiqui, S.I., Rathi, G., Chaudhry, S.A.: Acid washed black cumin seed powder preparation for adsorption of methylene blue dye from aqueous solution: thermodynamic, kinetic and isotherm studies. J. Mol. Liq. **264**, 275–284 (2018)
36. Khan, T.A., Chaudhry, S.A., Ali, I.: Equilibrium uptake, isotherm and kinetic studies of Cd(II) adsorption onto iron oxide activated red mud from aqueous solution. J. Mol. Liq. **202**, 165–175 (2015)
37. Ardejani, F.D., Badii, K.H., Yousefi Limaee, N., Shafaei, S.Z., Mirhabibi, A.R.: Adsorption of direct red 80 dye from aqueous solution onto almond shells: effect of pH, initial concentration and shell type. J. Hazard. Mater. **151**, 730–737 (2008)
38. Ay, Ç., Özcan, A.S., Erdoğan, Y., Özcan, A.: Characterization and lead (II) ions removal of modified Punica granatum *L. peels*. Int. J. Phytoremediation **19**, 327–339 (2017)
39. Kerkez, Ö., Bayazit, Ş.S.: Magnetite decorated multi-walled carbon nanotubes for removal of toxic dyes from aqueous solutions. J. Nanoparticle Res. **16**, 2431 (2014)
40. Tan, Y., Chen, M., Hao, Y.: High efficient removal of Pb(II) by amino-functionalized Fe_3O_4 magnetic nano-particles. Chem. Eng. J. **191**, 104–111 (2012)
41. Beyki, M.H., Fazli, Y.: Polyhydroxyquinoline-carbon nanotube chelating resin for selective adsorption of lead ions: multivariate optimization, isothermic, and thermodynamic study. Res. Chem. Intermed. **43**, 737–754 (2017)
42. Boparai, H.K., Joseph, M., O'Carroll, D.M.: Kinetics and thermodynamics of cadmium ion removal by adsorption onto nano zerovalent iron particles. J. Hazard. Mater. **186**, 458–465 (2011)
43. Siddiqui, S.I., Chaudhry, S.A.: A review on graphene oxide and its composites preparation and their use for the removal of As^{3+} and As^{5+} from water under the effect of various parameters:

application of isotherm, kinetic and thermodynamics. Process Saf. Environ. J. **119**, 138–163 (2018)
44. Mostafa, M., Chen, Y.H., Jean, J.S., Liu, C.C., Lee, Y.C.: Kinetics and mechanism of arsenate removal by nanosized iron oxide-coated perlite. J. Hazard. Mater. **187**, 89–95 (2011)
45. Khorzughy, S.H., Eslamkish, T., Doulati Ardejani, F., Heydartaemeh, M.R.: Cadmium removal from aqueous solutions by pumice and nano-pumice. Korean J. Chem. Eng. **32**, 88–96 (2015)
46. Shan, R.R., Yan, L.G., Yang, K., Hao, Y.F., Du, B.: Adsorption of Cd(II) by Mg^{-} Al^{-} CO_3^{-} and magnetic Fe_3O_4/Mg^{-} Al^{-} CO_3^{-} layered double hydroxides: kinetic, isothermal, thermodynamic and mechanistic studies. J. Hazard. Mater. **299**, 42–49 (2015)
47. Mallakpour, S., Behranvand, V.: Water sanitization by the elimination of Cd^{2+} using recycled PET/MWNT/LDH composite: morphology, thermal, kinetic, and isotherm studies. ACS Sustain Chem. Eng. **5**, 5746–5757 (2017)
48. Sun, W., Jiang, B., Wang, F., Xu, N.: Effect of carbon nanotubeson Cd(II) adsorption by sediments. Chem. Eng. J. **264**, 645–653 (2015)
49. Tiwari, A., Sharma, N.: Kinetic and thermodynamic studies of adsorption of Cd^{2+} by superparamagnetic nano iron oxide-loaded poly(acrylonitrile-Co-acrylic acid) hydrogel. Res. Chem. Intermed. **41**, 2043–2062 (2015)
50. Tran, H.N., You, S.-J., Chao, H.-P.: Thermodynamic parameters of cadmium adsorption onto orange peel calculated from various methods: a comparison study. J. Environ. Chem. Eng. **4**, 2671–2682 (2016)
51. Kataria, N., Garg, V.: Green synthesis of Fe_3O_4 nanoparticles loaded sawdust carbon for cadmium (II) removal from water: regeneration and mechanism. Chemosphere **208**, 818–828 (2018)
52. Chansuvarn, W., Pandee, Y., Saechim, A., Habumee, K.: Adsorption of cadmium (II) ion from aqueous solution onto a raw material of bamboo powder and its surface modification. Appl. Mech. Mater. **879**, 131–136 (2018)
53. Borah, R., Gogoi, A., Biswas, S., Goswami, R., Shim, J., Ara Begum, N., Kumar, M.: Efficacy and field applicability of Burmese grape leaf extract (BGLE) for cadmium removal: an implication of metal removal from natural water. Ecotox. Environ. Saf. **147**, 585–593 (2018)
54. Xiong, T., Yuan, X., Chen, X., Wu, Z., Wang, H., Leng, L., Wang, H., Jiang, L., Zeng, G.: Insight into highly efficient removal of cadmium and methylene blue by eco-friendly magnesium silicate-hydrothermal carbon composite. Appl. Surf. Sci. **427**, 1107–1117 (2018)
55. Li, R., Liang, W., Huang, H., Jiang, S., Guo, D., Li, M., Zhang, Z., Ali, A., Wang, J.J.: Removal of cadmium (II) cations from an aqueous solution with aminothiourea chitosan strengthened magnetic biochar. J. Appl. Polym. Sci. **135**, 46239–46246 (2018)
56. Qu, J., Meng, X., Jiang, X., You, H., Wang, P., Ye, X.: Enhanced removal of Cd (II) from water using sulfur-functionalized rice husk: characterization, adsorptive performance and mechanism exploration emperature = 25°C. J. Clean. Prod. **183**, 880–886 (2018)